Supporting Information

Electronic Structure Modulation in Ag Nanoparticle-$Ag_2Cu_2O_3$ Catalyst: A strategy for Stable and Enhanced Oxygen Reduction Reaction

Anagha Yatheendran[a], Dhakshina Prakash[a], Mohammed Ibrahim Shah M A[a], Maitreyo Biswas[b], Arun Mannodi-Kanakkithodi[b] and N. Sandhyarani[a]*

[a]*Nanoscience Research Laboratory, Department of Materials Science and Engineering, National Institute of Technology Calicut, Calicut, Kerala, India, Fax: 91 495 2287250, Tel.: 91 495 2286537, * E-mail: sandhya@nitc.ac.in*
[b]*School of Materials Engineering, Purdue University, West Lafayette, IN 47907, USA*

Synthesis of control materials

Composite synthesised with a 1:2 precursor ratio

A 0.01 M $AgNO_3$ and 0.02 M copper acetate monohydrate were dissolved in 50 mL DI water under vigorous stirring. Then, 50 mL of 5 M NaOH was added slowly to the above solution and stirred further for 40 min. The precipitate obtained was washed several times with DI water and ethanol, dried at 80 °C, and collected.

Composite synthesised with a 2:1 precursor ratio

A 0.02 M $AgNO_3$ and 0.01 M copper acetate monohydrate were dissolved in 50 mL DI water under vigorous stirring. Then, 50 mL of 5 M NaOH was added slowly to the above solution and stirred further for 40 min. The precipitate obtained was washed several times with DI water and ethanol, dried at 80 °C, and collected.

Ag-Cu MTMO

The in-situ derived Ag-Cu oxide was synthesised through the coprecipitation method. Separate solutions of 0.05 M silver nitrate and 0.025 M copper acetate monohydrate were prepared, and the copper acetate solution was added dropwise to the silver nitrate solution under stirring. Stirring was continued for 10 min and 1 M NaOH was added dropwise to the solution mixture to adjust the pH to 10. The resulting solution was stirred further for 40 min and the final product was collected after centrifugation and drying at 80 °C.

Ag_2O-CuO

The ex-situ derived composite was synthesized by mixing separately prepared Ag_2O and CuO in 15 mL solutions each followed by stirring for 40 min and the final product was collected after centrifugation and drying at 80 °C.

CuO

CuO was synthesized using copper acetate monohydrate treated with NaOH. 15 mL 0.025 M copper acetate solution was prepared initially and NaOH was added upon stirring. The stirring was further continued for 40 min and washed with DI water. The precipitate obtained after purification was dried at 80°C.

The complete conversion of $Cu(OH)_2$ was possible with calcination at 500 °C for 3 h.

Ag_2O

The silver oxide Ag_2O was synthesized from silver nitrate and NaOH was used as a reducing agent. 15 mL 0.05 M $AgNO_3$ solution was prepared initially and NaOH was added upon stirring. The stirring was further continued for 40 min and washed with DI water. The precipitate obtained after purification was dried at 80 °C.

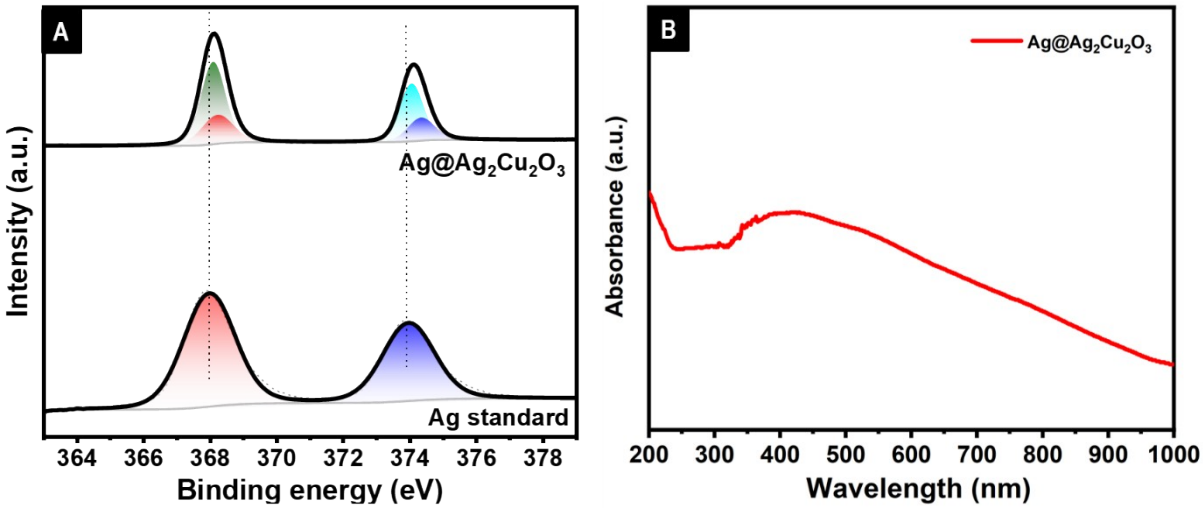

Fig. S1. Ag 3d region of $Ag@Ag_2Cu_2O_3$ along with the standard Ag (A), and UV-Vis absorption spectrum of $Ag@Ag_2Cu_2O_3$ (B).

UV-Vis absorption spectrum confirms the existence of silver nanoparticles with the presence of surface plasmon resonance peak of silver nanoparticles around 420 nm.

ORR activity of $Ag@Ag_2Cu_2O_3$

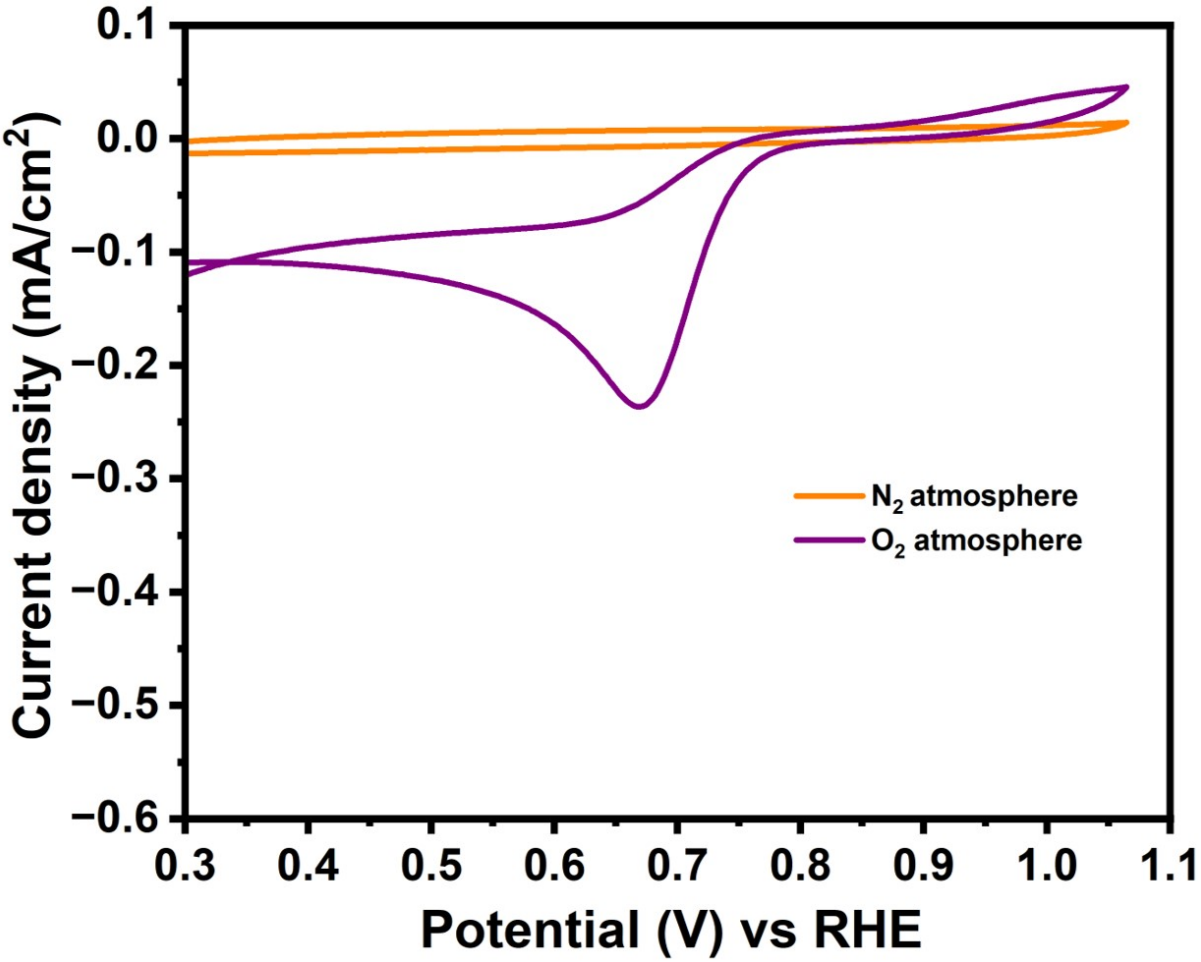

Fig. S2. Cyclic voltammogram of $Ag@Ag_2Cu_2O_3$ in N_2 and O_2 saturated solution

ECSA of $Ag@Ag_2Cu_2O_3$

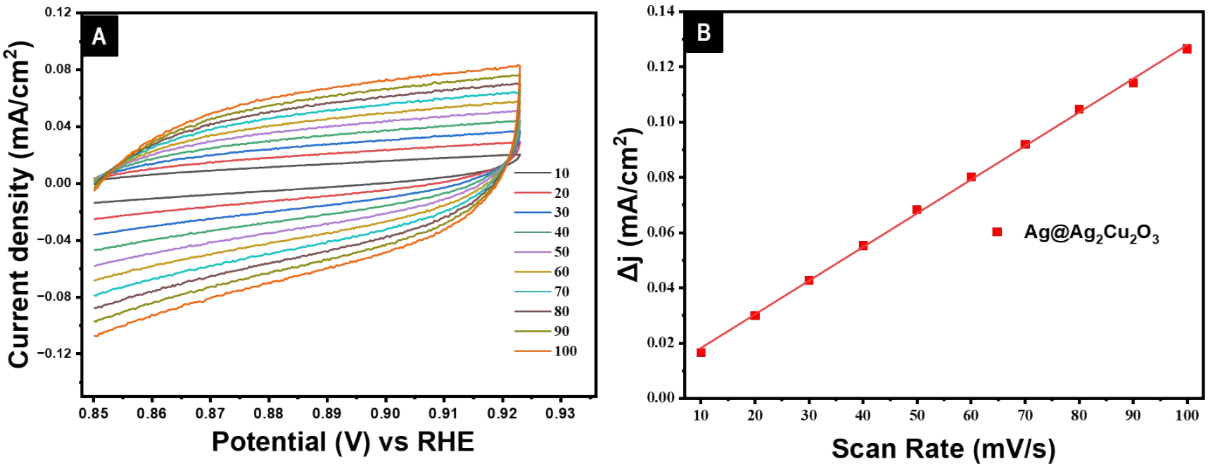

Fig. S3. The CV curve ranges from 0.85 to 0.92V (vs RHE) in a nitrogen-saturated environment using 0.1 M NaOH, with a scan rate varying between 10 and 100 mV/s (A), Difference of charge density Vs Scan rate of $Ag@Ag_2Cu_2O_3$ (B).

The slope is used to determine the double-layer capacitance (C_{dl}). The equation for ECSA is presented as follows,

$$\text{ECSA} = \frac{C_{dl}}{C_s}$$

The double-layer capacitance (Cdl) is determined from the slope of the charge difference versus scan rate plot, yielding a value of 0.6 mF. The specific capacitance (Cs) is calculated to be 0.004 mF/cm². Based on these calculations, the electrochemically active surface area (ECSA) of $Ag@Ag_2Cu_2O_3$ is determined to be 15 cm².

Characterisation of catalysts prepared with different ratios of precursors

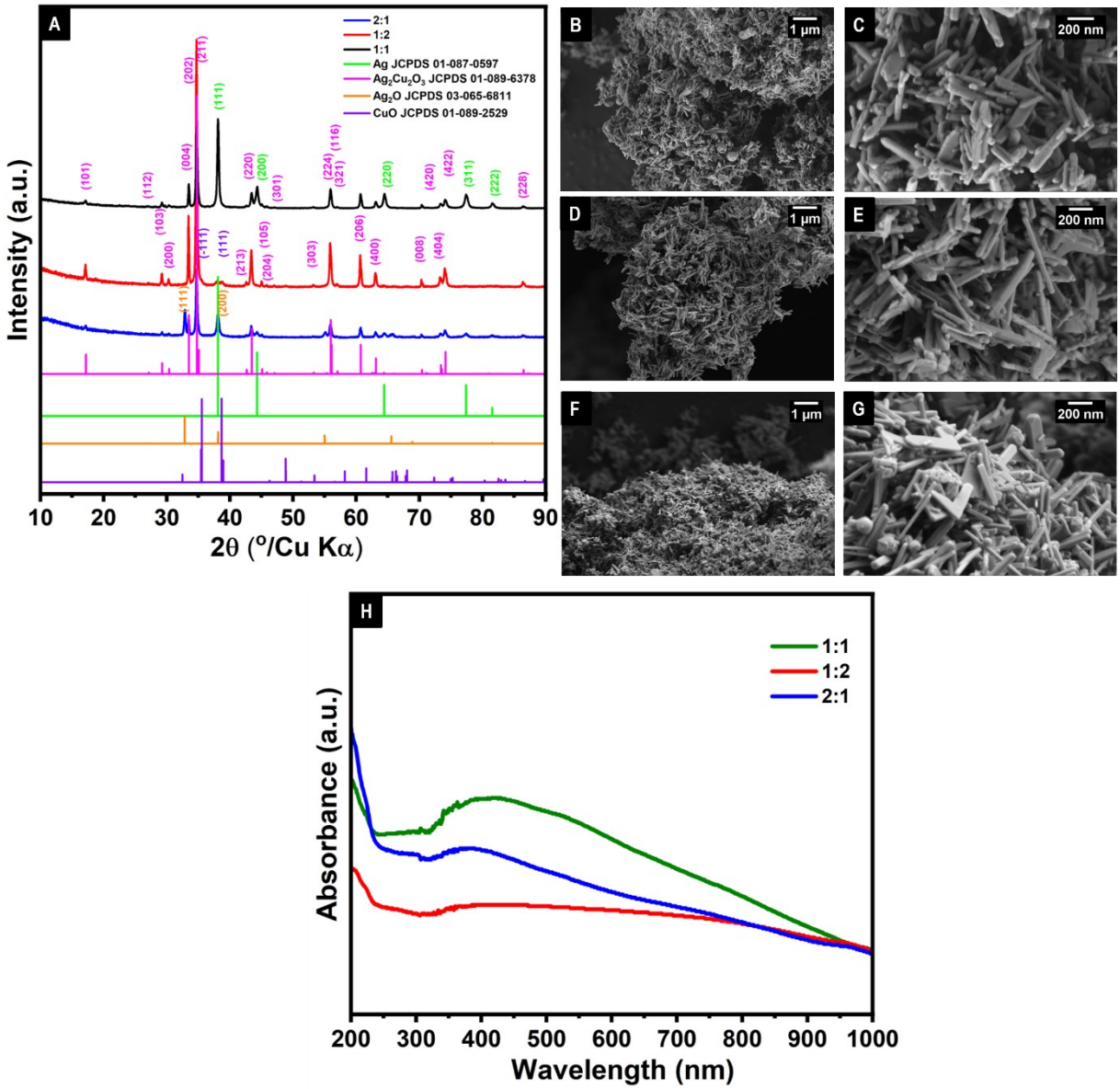

Fig. S4. Comparison of XRD (A) and SEM images of catalysts prepared with different ratios of precursors (1:1) (B-C), (1:2), (D-E), and 2:1 (F-G). UV-VIS spectrum of the three composites (H)

Characterisation of in-situ and ex-situ synthesised composite

The in-situ single-step synthesis with a lower concentration of NaOH (1M) results in a composite of Ag_2O and CuO with a small extent of Ag and $Ag_2Cu_2O_3$ and is represented here as Ag-Cu MTMO. The ex-situ synthesis resulted in the formation of Ag_2O and CuO, represented as Ag_2O-CuO.

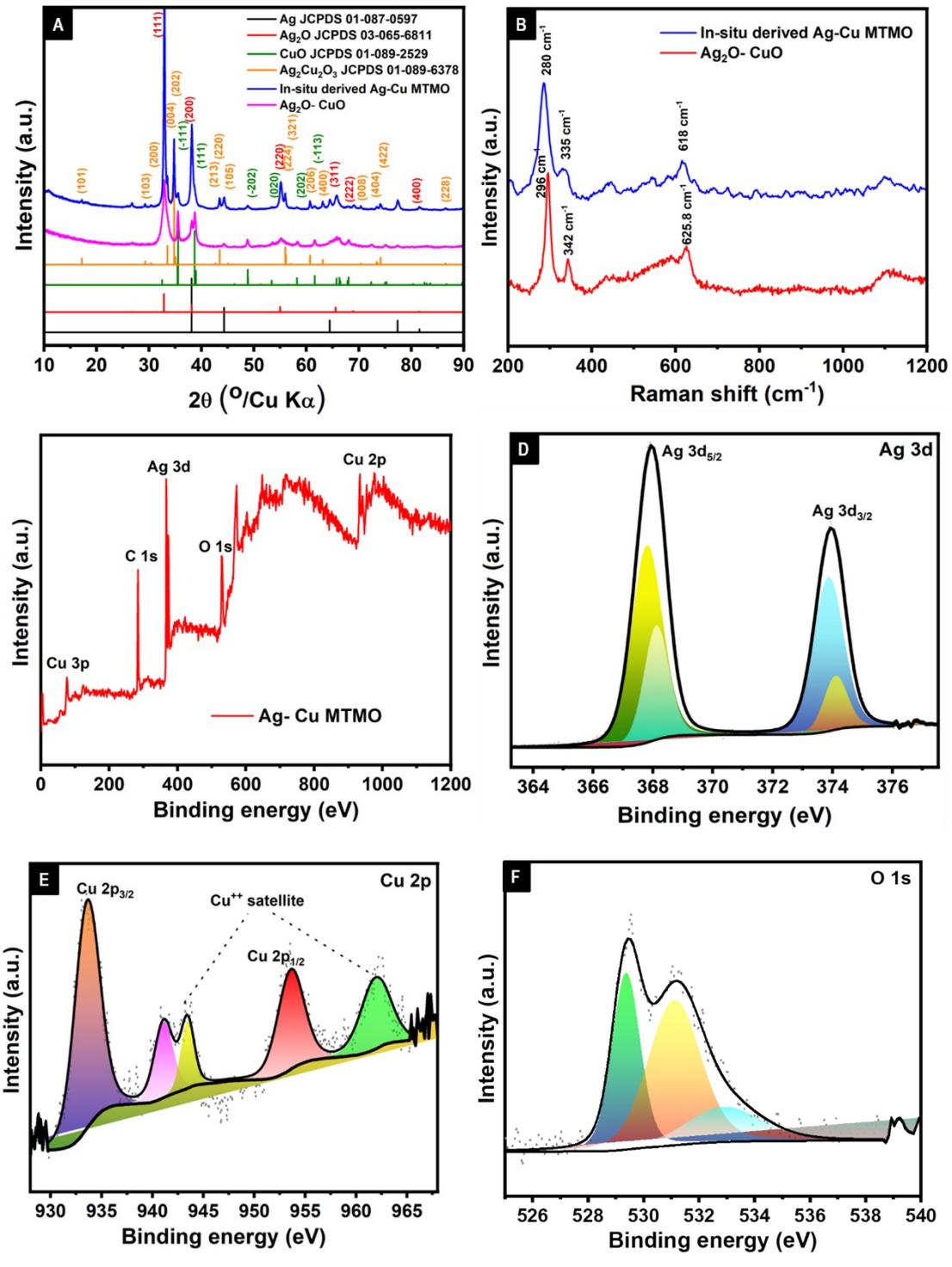

Fig. S5. XRD (A) and Raman (B) of in-situ, and ex-situ synthesized catalysts, XPS spectrum of Ag-Cu MTMO (C), XPS of in-situ derived Ag-Cu MTMO in the regions Ag 3d (D), Cu 2p (E), O 1s (F).

The XRD pattern of in-situ and ex-situ derived electrocatalysts with JCPDS of all the reference materials are given in Figure S5A. The XRD analysis revealed the formation of Ag_2O as the major component along with CuO, Ag, and a small extent of mixed silver copper oxide $Ag_2Cu_2O_3$ in the In-situ synthesis. The high-intensity diffraction peaks corresponding to Ag_2O are observed at 26.7°, 32.9°, 38.1°, 47.1°, 55.1°, 65.8°, 69°, 75.2°, 81.5°, 84.7° can be attributed to the (110), (111), (200), (211), (220), (311), (222), (321), (400), and (322) planes of cubic silver oxide (Ag_2O) with JCPDS 03-065-6811. The existence of monoclinic CuO was confirmed with the presence of characteristic peaks at 35.5°, 48.7°, 53.3°, 58.2°, 61.5°, 65.8°, 68.2°, 69°, 72.3°, 75.2°, and 86.4° corresponding to (-111), (-202), (020), (202), (-113), (022), (220), (-221), (311), (-222), and (-402) planes of monoclinic CuO (01-089-2529). A small extent of $Ag_2Cu_2O_3$ formation was also observed with XRD and characteristic low intense peaks were observed at 17.2°, 29.3°, 30.3°, 33.5°, 34.7°, 42.6°, 43.4°, 45°, 47.1°, 53.3°, 55.2°, 55.9°, 57°, 60.7°, 63.1°, 64.4°, 65.8°, 70.3°, 73.3°, 74°, 81.5°, and 86.4°, which are attributed to the (101), (103), (200), (004), (202), (213), (220), (105), (301), (303), (215), (224), (321), (206), (400), (305), (411), (008), (404), (422), (425), and (228) planes of tetragonal $Ag_2Cu_2O_3$ with JCPDS 01-089-6378. The XRD of the ex-situ derived catalyst exhibited all the characteristic peaks of Ag_2O, and CuO, and no additional peaks were present, confirming the absence of integrated mixed transition metal oxide structures.

Raman spectra of in-situ and ex-situ derived catalysts are shown in Figure S5B. Three major characteristic peaks corresponding to CuO were observed in both the catalysts, with peaks at 280 cm^{-1} (A_g mode), 335 cm^{-1} ($B_g^{(1)}$ mode), and 618 cm^{-1} ($B_g^{(2)}$ mode) in the in-situ derived catalyst, and a slight shift in peak position is observed in ex-situ derived Ag_2O-CuO. The characteristic peaks in the Ag_2O-CuO composite were observed at 296 cm^{-1} (A_g mode), 342 cm^{-1} ($B_g^{(1)}$ mode), and 625.8 cm^{-1}($B_g^{(2)}$ mode).

To analyze the composition in detail, XPS was performed for the in-situ derived Ag-Cu MTMO catalyst, and the spectra in the Ag 3d, Cu 2p, and O 1s regions are shown in Figures S5 D-F, with the wide scan spectrum provided in SI, Figure S5 C. The Ag 3d region (Figure S5D) can be deconvoluted with characteristic peaks at 367.8 and 373.8 eV, attributed to the Ag^+ state in Ag_2O and $Ag_2Cu_2O_3$. The presence of an Ag^0 oxidation state at 368.1, 374.1 eV confirms the surface occupation of silver nanoparticles. The Cu 2p XPS spectrum shown in Figure S5E reveals deconvoluted peaks at 933.5 and 953.5 eV corresponding to the Cu^{2+} oxidation state with a separation of 20 eV. Shake-up peaks were present at 941.1, 943.4, and 971.9 eV, confirming the existence of Cu (II). The deconvoluted XPS spectrum of O1s is given in Figure S5F. The spectrum exhibited characteristic peaks at 529.3, 531.1,

and 532.8 eV that can be attributed to the oxygen from the Ag_2O, the hydroxyl group, and water adsorbed on the surface.

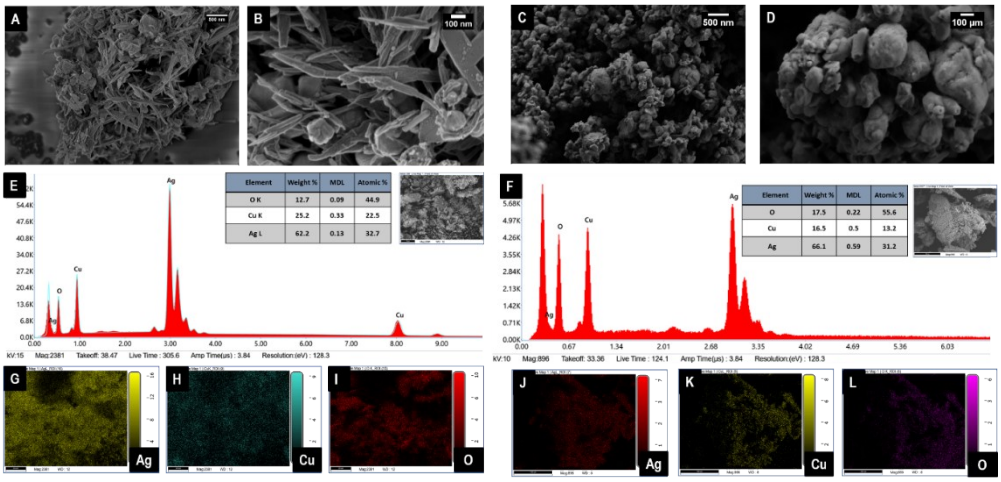

Fig. S6. SEM images of in-situ (A, B), ex-situ (C, D) catalysts, EDS spectrum, and mapping of in-situ (E, and G-I), ex-situ (F, J-L).

Morphological analysis of both the in-situ and ex-situ derived catalysts was performed using SEM, and the results obtained are shown in Figures S6A, B, and C, D with higher and lower magnifications, respectively. A mixed morphology was observed in the SEM of the in situ-derived sample, while a bulk particle agglomerated kind of morphology was observed in the Ag_2O-CuO composite. The energy-dispersive X-ray spectroscopy portrayed in Figure S6E, F confirms the existence of silver, copper, and oxygen in in-situ derived Ag-Cu MTMO and Ag_2O-CuO. The distribution of elements is displayed with the EDS mapping shown in Figures S6G-I, and S6J-L for the in-situ derived integrated catalytic system and ex-situ derived composite.

ORR activity of all the catalysts

ORR activity of Ag-Cu MTMO, Ag_2O-CuO, Ag_2O, CuO, and Ag@$Ag_2Cu_2O_3$ are compared at 2600 rpm and the LSV is given in figure S7.

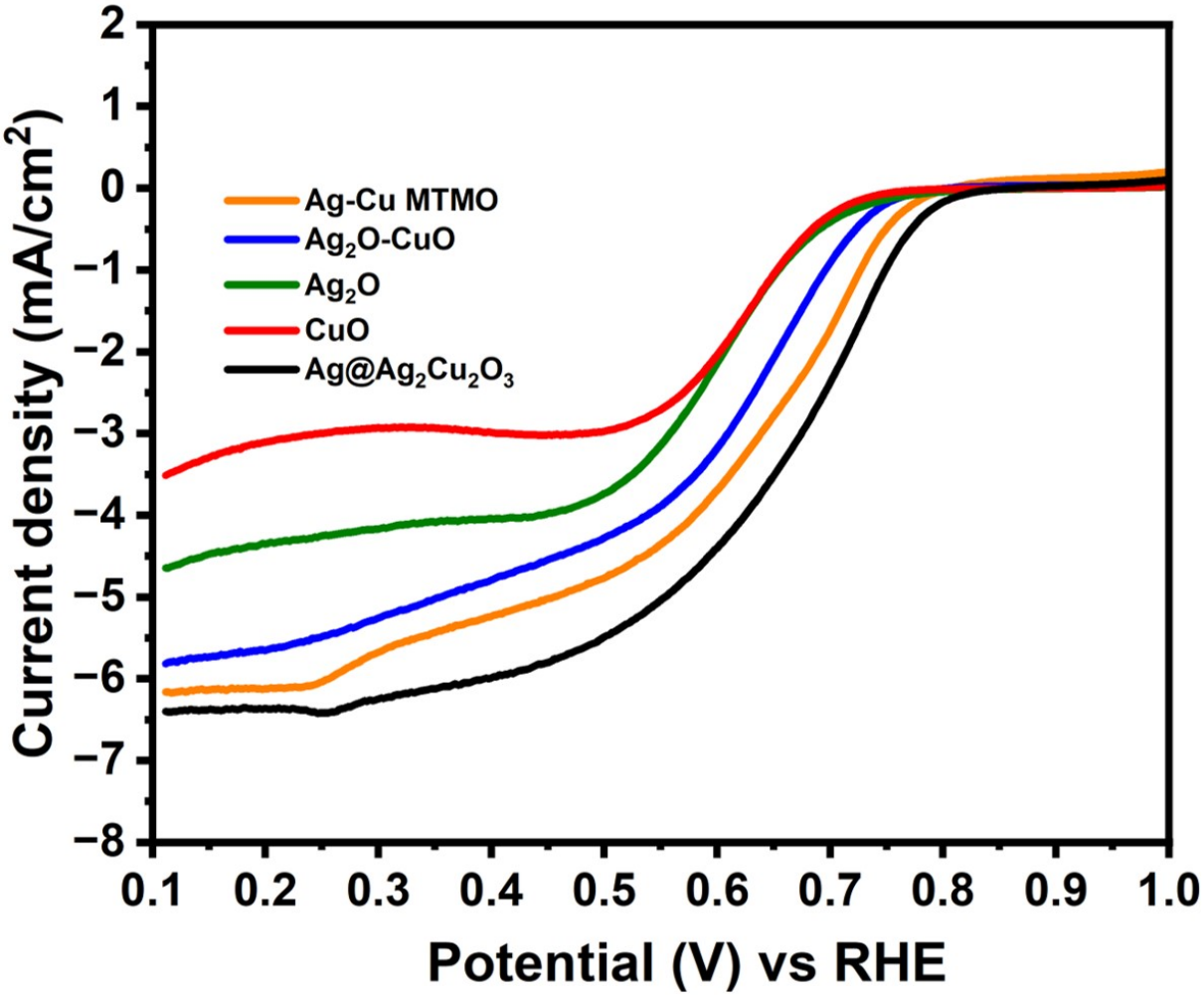

Fig. S7. Comparison of LSV of Ag-Cu MTMO, Ag_2O-CuO, Ag_2O, CuO, and Ag@$Ag_2Cu_2O_3$ at 2600 rpm.

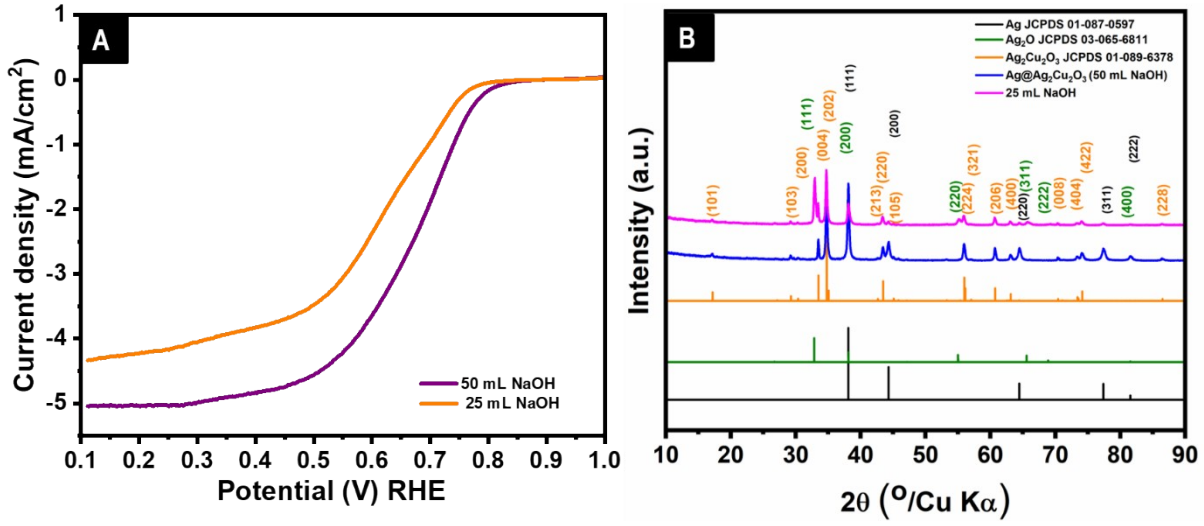

Fig. S8. Comparison of LSV (A) and XRD (B) of catalysts derived with different volumes of NaOH at 2000 rpm

We have analysed the ORR activity of catalytic systems with different extents of Ag and $Ag_2Cu_2O_3$ formation. The system derived from an equimolar mixture of silver and copper precursors shows enhanced activity. The greater concentration of silver precursor results in Ag_2O formation, and the copper precursor results in CuO formation. Similarly, a comparison is performed with different volumes of 5 M NaOH, and it is observed that a lower volume results in reduced generation of the mixed oxide phase, and, in addition, an Ag_2O phase forms. On comparing the activity, it is observed that the catalytic system with a greater contribution from silver nanoparticles and mixed oxide shows greater activity due to a synergistic effect than a single metal oxide.

ADT analysis of Ag- Cu MTMO (A), and Ag_2O-CuO

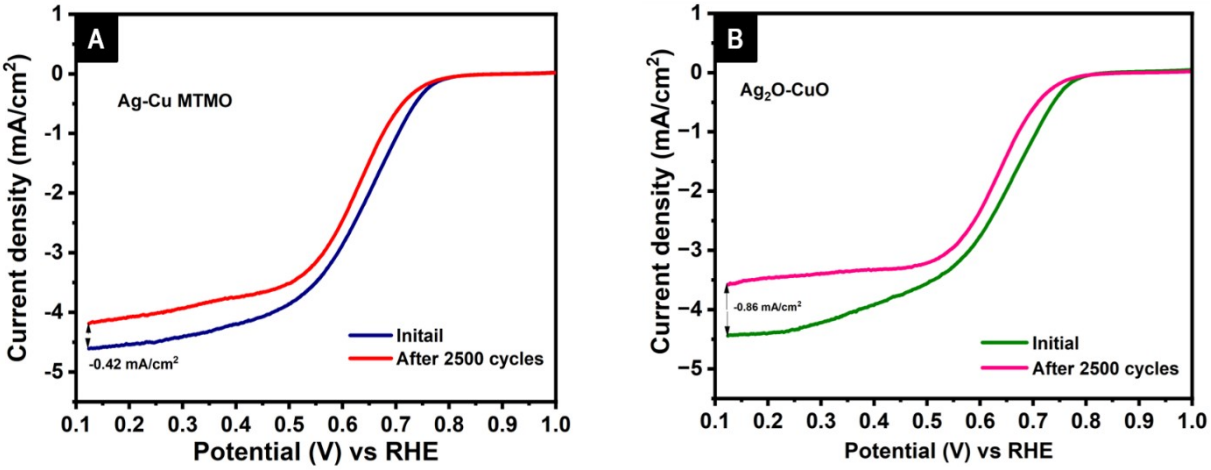

Fig. S9. Stability study of Ag- Cu MTMO (A), and Ag_2O-CuO (B) (1600 rpm).

The in-situ derived mixed oxide composite exhibited excellent stability, with minimal reduction in current density (ΔI = -0.42 mA/cm^2) after 2500 continuous CV cycles. Similarly, the ex-situ derived physically mixed Ag_2O-CuO catalyst exhibited a visible reduction (ΔI = -0.86 mA/cm^2) compared to the integrated system, confirming the role of an integrated catalytic system for long-term fuel cell application.

Post-ADT characterisations of Ag@$Ag_2Cu_2O_3$

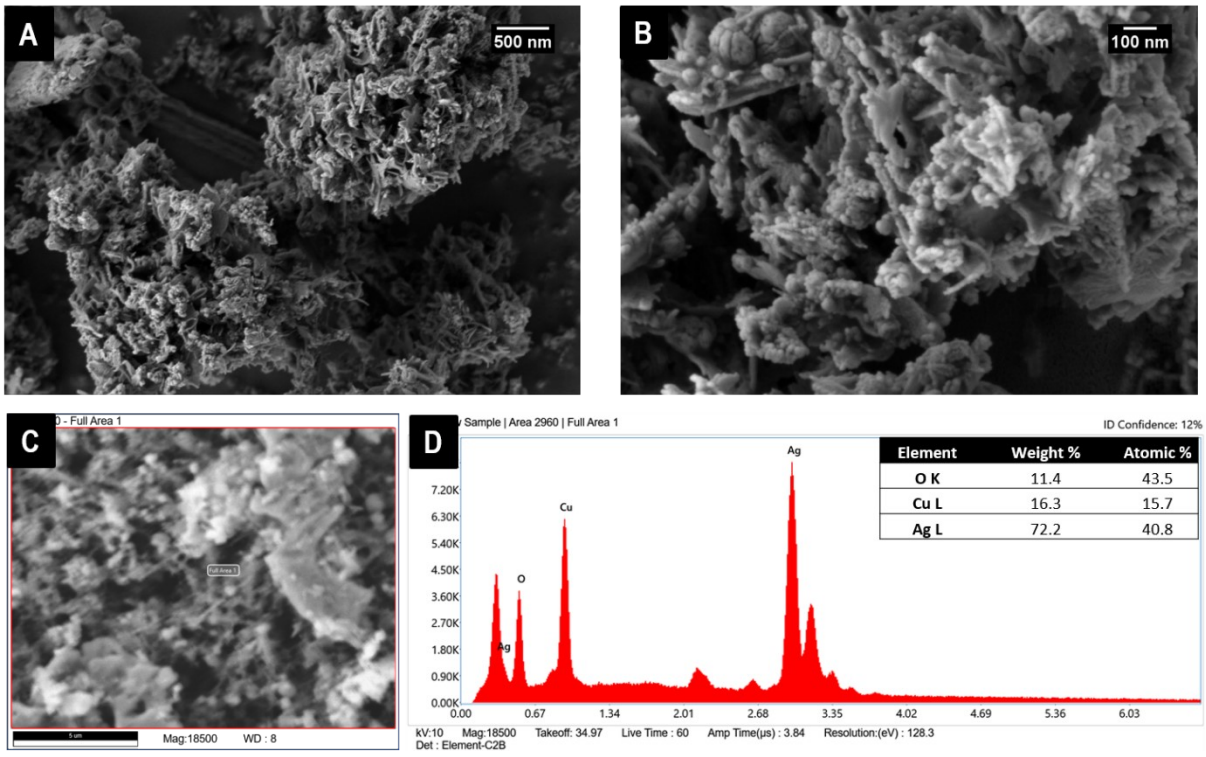

Fig. S10. SEM images (A, B), Electronic image (C), and EDS spectrum with percentage atomic distribution (D) after ADT analysis of the catalyst

SEM and EDS spectrum, with elemental composition, of the catalyst after ADT analysis, are shown in Figure S10. There was a reduction in the homogeneous distribution of nanorods corresponding to $Ag_2Cu_2O_3$ after ADT, with a higher proportion of anchored spherical Ag nanoparticles. The increase in the composition of Ag is confirmed with EDS after ADT, which is in accordance with XRD and XPS results.

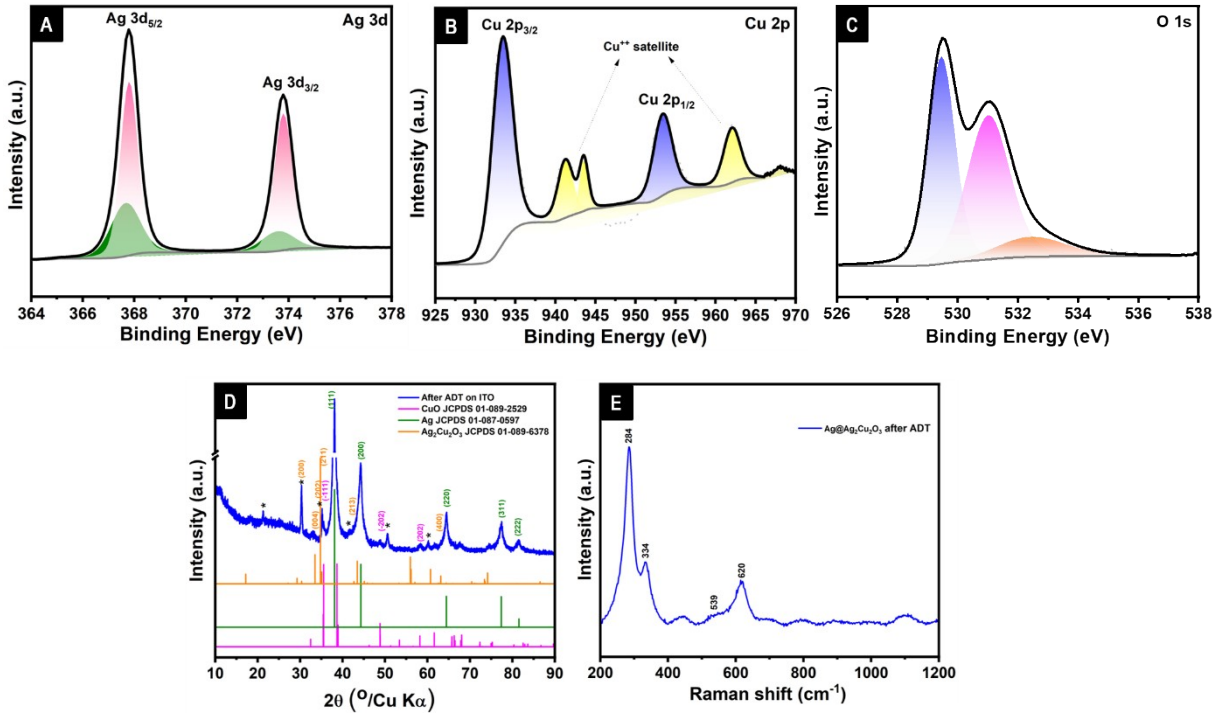

Fig. S11. XPS of Ag 3d (A), Cu 2p (B), O 1s (C) regions after ADT, XRD pattern (D), and Raman spectrum (E) after ADT analysis

The distinctive peaks of deconvoluted Ag 3d (Figure S11 A) present two lower area peaks at 367.6 and 373.5 eV, which can be attributed to the Ag (+) oxidation state from the $Ag_2Cu_2O_3$ and two intense higher area peaks present at 367.8 and 373.79 eV indicate the presence of Ag (0) after the conversion in ADT. The deconvoluted Cu 2p XPS (Figure S11 B) indicated the peaks at 933.4 and 953.4 eV, along with pronounced shake-up peaks confirming the presence of Cu (II) oxidation states. The deconvoluted oxygen XPS spectrum (Figure S11 C) indicates the presence of two distinctive peaks at 529.4 and 531 eV, which can be attributed to the two lattice oxygens, and the peak at 532.46 eV that indicates the presence of physisorbed or chemisorbed water molecules on the surface. XRD analysis is performed after ADT (Figure S11 D) on the catalyst-coated ITO substrate. To obtain the uniform coating for XRD analysis, the catalyst ink was prepared with a 5 mg / 1 mL ratio, and 200 µL of the catalyst ink was drop-cast on a 1*1 area of the ITO plate. The characteristic peaks corresponding to ITO plates are indicated in the figure. After the ADT analysis, the intensity of characteristic peaks corresponding to Ag increases with a reduction in the intensity of peaks corresponding to $Ag_2Cu_2O_3$. The characteristic peaks present at 38.1°, 44.2°, 64.4°, 77.4°, and 81.4° correspond to (111), (200), (220), (311), and (222) planes of Ag with JCPDS 01-087-0597. The characteristic peaks observed at 30.3°, 33.3°, 34.7°, 35.1°, 42.5°, and 63.1° are attributed to the (200), (004), (202), (211), (213), and (400) planes of tetragonal $Ag_2Cu_2O_3$ with JCPDS 01-089-6378. Low-intensity peaks corresponding to CuO were also observed at 35.5°, 48.9°, and 58.3° that belong to (-111), (-202), and (202) planes of CuO with JCPDS 01-089-2529.

The Raman analysis is performed after 2500 CV cycles of ADT, and the sample exhibited peaks corresponding to Cu-O stretching at 284, 334, and 620 cm^{-1}, respectively.

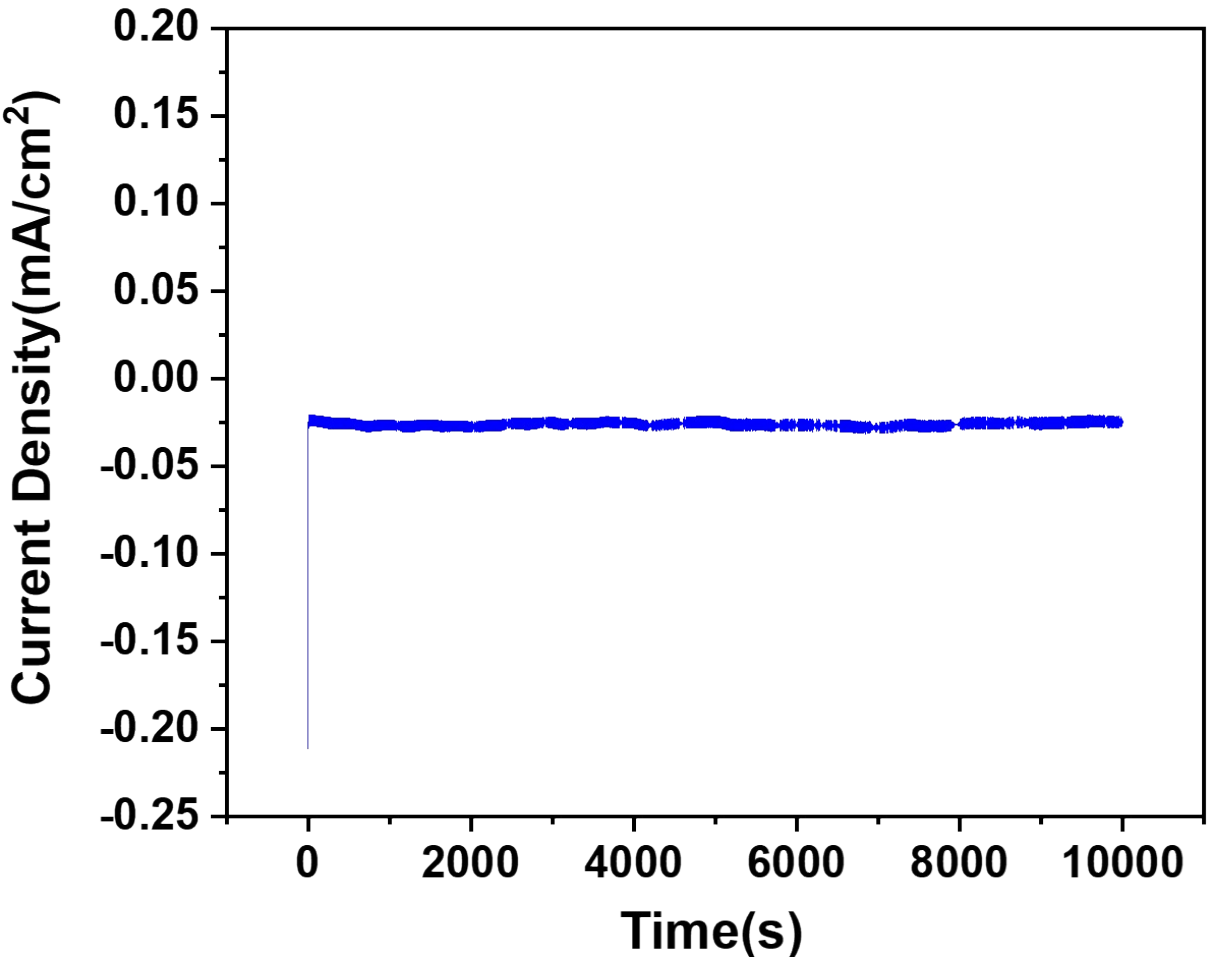

Fig. S12. Chronoamperometric analysis of the stability of Ag@ $Ag_2Cu_2O_3$

A systematic investigation of O* adsorption was performed for different surface slabs and different adsorption sites, with and without small Ag clusters on the $Ag_2Cu_2O_3$ (100) surface. O* adsorption on pristine Ag (111) and $Ag_2Cu_2O_3$ (100) surfaces were also analyzed to provide a comprehensive comparison of adsorption behavior relevant to the ORR mechanism. The adsorption energy (E_{ads}) of the oxygen molecule on the catalyst is quantified as follows:

$$E_{ads} = E_{surf+O} - E_{surf} - 1/2E_{O2}$$

Here, E_{surf+O} refers to the total energy of the surface slab system with the adsorbate and E_{surf} corresponds to the total energy of the clean surface slab before the addition of any oxygen. The possible positions for adsorption are given below in Figure S13.

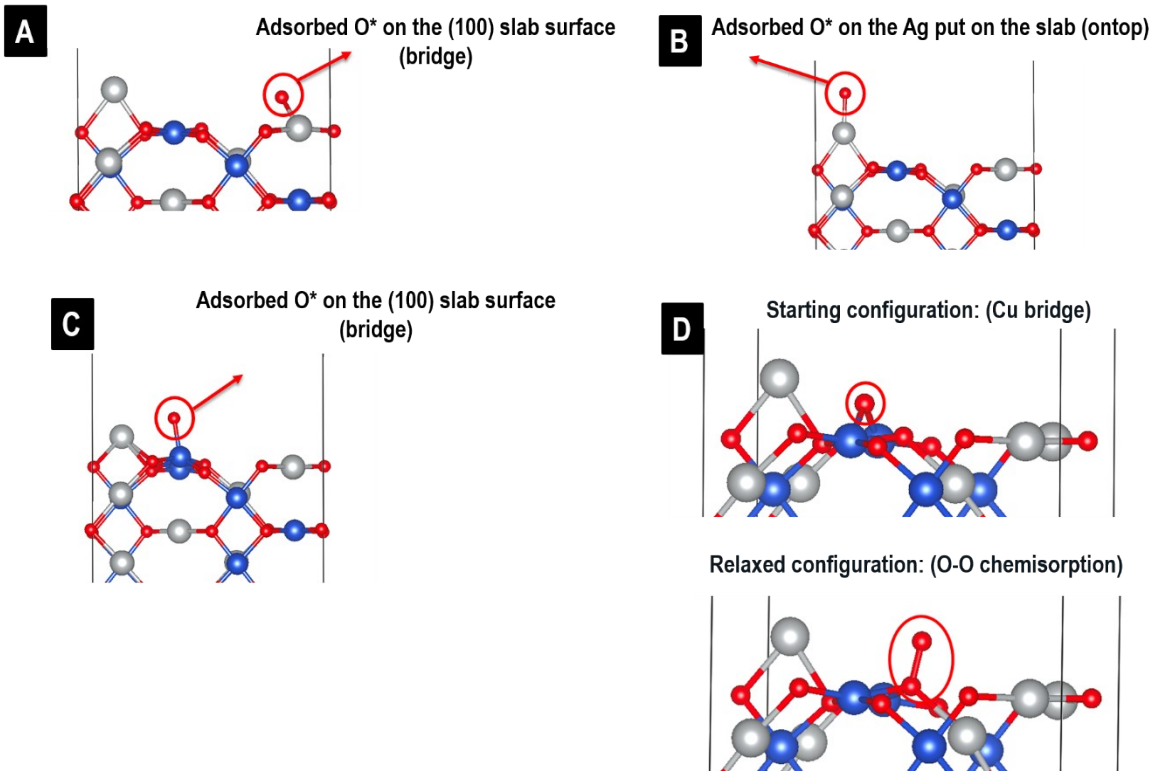

Fig S13: Possible O* adsorption sites on the AgNP and $Ag_2Cu_2O_3$ (100) surface.

Our results show that the Ag d-band center is closer to the Fermi level (E_F) for the $Ag_2Cu_2O_3$ (100) slab as compared to pristine Ag or $Ag_2Cu_2O_3$, and it is shifted 0.15 eV away from the E_F by the addition of an Ag atom on the (100) slab. While the O* adsorption is stronger on the added Ag atom on the slab than on the Ag atoms on the surface, it is in great agreement with the "spillover" mechanism. On the surface slab, we compared the O* adsorption energies at the Ag (bridge), Cu (ontop) and O (ontop) sites. Interestingly, we observed that starting from the Cu-bridge site, the chemisorbed O* drifted towards the O-site showing considerably lower adsorption energy (~0.5-0.6 eV) as compared to the

Ag (bridge), and Cu (ontop) sites. Thus, it is observed that the Ag NPadsorption is significantly more stable, and the adsorbed O* "spills over" to $Ag_2Cu_2O_3$ surface O-sites.

MEA Preparation

The Fumasep FAA-3-50 (7 × 7 cm^2) membrane was pre-treated before the fabrication of MEA. To replace the bromide ions in the membrane with hydroxyl groups in the polymer matrix, the membrane was soaked in 1 M NaOH for 24 hours and then rinsed several times. After the pretreatment, the membrane was kept in 1 M NaOH in a closed container to avoid CO_2 contamination. Gas diffusion layers (GDLs) of 5 × 5 cm^2 and gaskets of 7 × 7 cm^2 (with a 5 × 5 cm^2 central cut-out) were taken. The membrane electrode assembly (MEA) was constructed by interposing PtRu/C at the anode and $Ag@Ag_2Cu_2O_3$ at the cathode, separated by the Fumasep FAA-3-50 membrane, analogous to the fabrication of PtRu/C at the anode and Pt/C at the cathode as the standard configuration. Catalyst inks were prepared by first adding the catalyst in DI water to ensure wetting, followed by the addition of isopropyl alcohol and 10 wt.% Fumion in N-methyl pyrrolidone. The resulting ink was coated onto the GDL with a brush painting approach to achieve the mass loading of 4.5 mg/cm^2 at the anode and 4 mg/cm^2 at the cathode. The MEA was assembled by cold-pressing the anode and cathode onto the pre-treated Fumasep FAA-3-50 membrane under a pressure of 0.5 tons for 30 seconds. During the testing, oxygen was purged through the cathode side, while a 1 M methanol solution in 1 M NaOH was circulated through the anode side at a flow rate of 1 mL/min using a peristaltic pump. Before the OCV measurement, the MEA was activated by concurrently delivering methanol and oxygen into their respective compartments for two hours.

DMFC analysis of standard MEA prepared with PtRu/C at the anode and Pt/C at the cathode

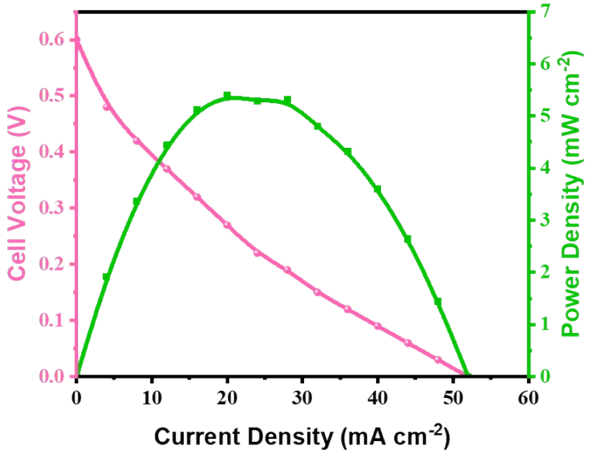

Fig. S14. Fuel cell performance analysis of standard MEA prepared with PtRu/C at the anode and Pt/C at the cathode

A comparative table summarising the DMFC performance of $Ag@Ag_2Cu_2O_3$ alongside recently reported catalysts operating under alkaline conditions is given below

SL No	Anode	Cathode	Concentration of Methanol	Operating Temperature	Collector	Current Density	Power Density	Reference
1.	1.5 mg/cm^2 (60% PtRu/C)	4 mg/cm^2 (Fe-N-C)	1M	40	Gold Plate	≈70 mA/cm^2	≈16 mW/cm^2	1.
2.	1 mg/cm^2 (20% Pt/C)	4 mg/cm^2 (5C-NP-Fe)	5 M	30	-	≈75 mA/cm^2	≈7 mW/cm^2	2.
3.	1.5 mg/cm^2 (75% PtRu/C)	4 mg/cm^2 (Pt-Fe-N-C)		60	Gold Plate	≈100 mA/cm^2	≈23 mW/cm^2	3.
4.	4 mg/cm^2 (sPdNiA)	4 mg/cm^2 (sPdNiA)	5 M	40	-	≈140 mA/cm^2	≈23 mW/cm^2	4.
5.	-	4 mg/cm^2 (Fe-N-C-2)	1 M	60	Stainless steel plates (316L, 0.45 mm thickness) with 200 nm Au layers deposited on the surface	≈130 mA/cm^2	≈16 mW/cm^2	5.
6.	3.75 mg/cm^2 (20% Pt/C)	5 mg/cm^2 (Co_1Fe_1@ NCNF/BCNT)	3M	40	-	≈120 mA/cm^2	≈7 mW/cm^2	6.
7.	1.5 mg/cm^2 (60% PtRu/C)	1 mg/cm^2 (Fe-N-C-1000)	5 M	60	-	≈180 mA/cm^2	≈50 mW/cm^2	7.
8	4.5 mg/cm^2 (30% PtRu/C)	4 mg/cm^2 ($Ag@Ag_2Cu_2O_3$)	1 M	40	Copper	≈48 mA/cm^2	≈5 mW/cm^2	This Work

Table 1: Comparison of DMFC performance in alkaline conditions

References

1. C. Lo, X. Lyu, I. Gatto, B. Zulevi, A. Serov and V. Baglio, Performance investigation of alkaline direct methanol fuel cell with commercial PGM-free cathodic materials *Journal of Power Sources,* **2023**, 561, 1–6, 232732.

2. D. Taxi, S. Shao, X. Maimaitiyiming, A. Sawut, M. Tursun, Z. Kuerban and H. Lin, Biomass carbon with defective structures as effective ORR catalyst for DMFC, *Sep. Purif. Technol*, 2025, 356, 129775.
3. G. A. Molina, C. L. Vecchio, V. Baglio, A.S. Aricò, E. Morallón, D. C. Amorós, Pt nanoparticles for improving the performance and durability of Fe-N-C based materials towards oxygen reduction reaction in alkaline direct methanol fuel cells, *Journal of Colloid and Interface Science*, **2025**, 691, 137426.
4. A. Sathyaseelan, V. Elumalai, K. Krishnamoorthy and A. Sajeev, Sphere-like PdNi Alloy: Unveiling the Twin Functional Properties toward Oxygen Reduction and Temperature-Dependent Methanol Oxidation for Alkaline Direct Methanol Fuel Cells, *ACS Sustainable Chem. Eng.* **2023**, 11, 5345−5355.
5. H. Deng, C. Hou, F. Ji and Y. Zhang, Zinc-assisted synthesis of Fe-N-C catalysts based on polyaniline with high oxygen reduction reaction catalytic activities in direct methanol fuel cells*Fuel Cells*, **2023**, 42–50.
6. S. Guo, S. Yu, F. Chen, L. Wang, M. Guo, T. Ren, C. Zhang and C. Li, Direct methanol fuel cell with enhanced oxygen reduction performance enabled by CoFe alloys embedded into N-doped carbon nanofiber and bamboo-like carbon nanotube, *J. Colloid Interface Sci.*, 2023, 652, 429–439.
7. S. Freitas, A. D. Epifanio, C. Lo, I. Gatto, V. Baglio, V. C. A. Ficca, E. Placidi and B. Mecheri, Tailoring MOF structure via iron decoration to enhance ORR in alkaline polymer electrolyte membrane fuel cells, *Chem. Eng. J.*, 2023, 465, 142987.